Influence of surface roughness on the sputter yield of Mo under keV D ion irradiation

M. Kelemen[1,2], T. Schwarz-Selinger[3], A. Mutzke[4], M. Balden[3], E. Vassallo[5], M. Pedroni[5], D. Dellasega[5,6], M. Passoni[5,6], F.Romeo[5,6], A. Hakola[7], P. Pelicon[1], R. Zaplotnik[1] and S. Markelj[1]

[1] Jožef Stefan Institute, Jamova 39, SI-1000 Ljubljana, Slovenia
[2] Jožef Stefan International Postgraduate School, Jamova cesta 39, 1000 Ljubljana, Slovenia
[3] Max-Planck-Institut für Plasmaphysik, Boltzmannstrasse 2, D-85748 Garching, Germany
[4] Max-Planck-Institut für Plasmaphysik, Wendelsteinstrasse 1, D-17491 Greifswald, Germany
[5] Istituto per la Scienza e Tecnologia dei Plasmi CNR, Via Roberto Cozzi, 53-20125 Milano, Italy
[6] Politecnico di Milano, via Ponzio 34/3, 20133 Milan, Italy
[7] VTT Technical Research Centre of Finland Ltd, P O Box 1000, FI-02044, VTT, Finland

***Corresponding author: Mitja Kelemen**

E-mail address: mitja.kelemen@ijs.si

The content of this manuscript is identical to an article with the same title published in Journal of Nuclear Materials Volume 555, November 2021, p. 153135

https://doi.org/10.1016/j.jnucmat.2021.153135

Abstract

In this work the influence of surface roughness on the sputter yield of Mo under keV D ion bombardment was investigated for different impact angles. For this purpose, thin films of Mo (~ 120 nm) were deposited by pulsed laser deposition onto graphite substrates with varying surface roughness (Ra ranging from 5 nm to 2-3 µm). The as-deposited samples were irradiated at room temperature by 3 keV D_3^+ ions originating from an electron cyclotron resonance ion gun. Samples were exposed to D ions at angles between 0° and 70° and fluences in range of 10^{23} D/m^2. The areal densities of the Mo marker layers were determined with Rutherford-backscattering spectroscopy. For all the surfaces we observed a strong angular dependence of the sputter yield. For smooth and intermediate surface roughnesses, up to Ra ~ 280 nm, we obtained an increase of the sputter yield with the angle up to a factor of five compared to 0°. In contrast, at the highest surface roughness in the 2-3 µm range the sputtering yield decreases with increasing impact angle. The obtained data were compared to SDTrimSP-3D simulations. We obtained good agreement between the simulated and experimental sputter yield for surfaces for which we could provide high resolution atomic force microscopy (AFM) surface representations. As high-resolution surface mapping was not possible for surface roughness of 2-3 µm, we found large deviation between the calculation and the measured data. The combination of measured and simulated data represent important input for predicting the erosion rates of surfaces in inner walls of thermonuclear fusion devices, which are expected to change surface roughness over time by sustained plasma exposure.

Keywords: Ion beam, Deuterium, RBS, Sputter yield, surface roughness, angular dependence

Introduction

An important issue in the development of thermonuclear fusion reactors is the lifetime of the reactor wall. Bombardment by energetic ions and neutrals from the plasma will lead to continuous erosion of the plasma-facing surface. In addition, the eroded material can contaminate the core plasma. Inside the plasma chamber of a fusion device, particles coming from the plasma impinge on the components at different angles depending on both local plasma parameters and on the orientation of the magnetic fields lines, which roughly guide the charged particles from plasma to the surface of the inner wall material. For instance at the components in the divertor region, the magnetic field lines intersect the target plate surface at shallow incidence angles of a few degrees. The particles impact at average angles of around 60°, with some angular distribution, due to the additional effect of the sheath potential on the ion trajectories close to the surface and additional gyration of ions in magnetic field [1].

Many studies have been carried out to determine the sputter yield on smooth surfaces in varying combinations of projectile ions and target atoms at different impact energies and impact angles. The major results are summarised in the work of *R. Behrisch and W. Eckstein* [2]. There a distinct angular dependence of the sputter yield is observed [2]. However, for rough surfaces the angular dependence can behave in an unexpected way [3-6] and most of the past work was done for materials (B, Fe), which are not presently foreseen in future fusion devices as plasma-facing materials. In general, the plasma-facing components (PFC) in a fusion device, which are affected by the highest particle fluxes (divertor), are made out of heavy refractory metals such as tungsten (W) [7]. For this reason, comparison between data extracted from well-defined laboratory experiments and results obtained in fusion devices is needed. In this paper we will concentrate on the first part.

The main goal of this study is to investigate the effect of surface roughness on sputter yield at different impact angles to improve the quality of the available data. In the past, some effort has been spent on the quantification of the sputter yields on rough surfaces in set-ups where a light projectile (H or D) impacted on a heavy target atom (heavier than Fe) [4,9]. Part of that work was focused on providing validation data for the development of computer codes such as SDTrimSP-3D [9] and TRI3DYN [8]. In the past studies, samples with well-defined surface topography and small values of surface roughness (up to 20 nm [5]) have been used. Data obtained in those studies are valuable for verifying the predictive quality of simulation codes. However, they are not representative for the surface topography of PFCs in a tokamak environment, which generally exhibit much higher roughness, even in their virgin condition as delivered from the material production line. To address this gap, we have decided to study erosion of thin Mo films on graphite substrate with varying degrees of surface roughness typical for tokamak PFCs. This study is a precursor for exposures in tokamak devices on similar surfaces. These tests are envisaged in ASDEX Upgrade (AUG). As AUG is a full W machine, the deposition of W from other plasma-facing components is unavoidable. To be able to observe the sputtering in AUG, a proxy material for W has to be chosen. Mo was chosen as both materials show similar behaviour of sputter yield under keV D ion bombardment [1,8], at least for smooth surfaces at 0° impact angle. The main difference is in absolute values of sputter yields and sputter threshold energy. The particle energies hitting the PFCs in a fusion device are predominately ions in the eV energy range, however some particles can reach keV energies. As most of the light particles (D, T, He) will have energies even below the sputter threshold [2], sputtering will be dominated by the high energy ions and neutrals originating from core plasma.. High energy particles are produced by instabilities of core plasma as response to different mechanism of heating the plasma. Additional some energetic particles are produced in charge exchange reactions, which are able to reached the reactor inner wall. For this reason we have decided to study the effect of sputter yield on surface roughness in keV energy range.

We used 115-120 nm thick Mo films deposited by pulsed laser deposition on textured graphite substrates of varying surfaces roughness. The samples were exposed to D ions with energy of 1 keV/D, under impact angles between 0° and 70°. The erosion was characterised using Rutherford Backscattering Spectroscopy (RBS) as the main analysis tool. The surface morphology was carefully analysed with atomic force microscopy (AFM), confocal laser scanning microscopy (CLSM) and scanning electron microscopy (SEM). Finally, SDTrimSP-3D simulations were performed and will be compared to the experimental data.

2. Sample preparation and characterization

For all studied samples, fine-grained graphite was used as substrate. The graphite was cut into 4 mm thick pieces of dimensions of 15×16 mm^2. Samples with four different surface roughness were prepared. As a measure for the surface roughness, we took the arithmetic average deviation from the average surface height, Ra, as measured by AFM or CLSM. The surface roughness of the samples ranged from polished surfaces (Ra~5 nm) up to very rough surfaces (Ra~2-3 μm, typical for a surface after machining), with two intermediate roughness steps of Ra~110 nm and Ra~280 nm. The samples were first polished to a surface roughness of Ra~5 nm, as measured with AFM, on a micrometer lateral scale. Fine grain graphite poses unique challenges during its polishing. Due to its grainy structure, some grains fell out during the polishing and the subsequent cleaning. This results many micrometer holes on the surface in the overall smooth surface. These influence the results, which will be elaborated in the discussion part of the paper.

Part of the polished substrates were then treated with plasma etching by exposing them to a plasma consisting of a mixture of CF_4 and H_2 gas at 9 Pa, driven with a 13.56 MHz RF power supply. To achieve Ra~110 nm, samples were exposed for 25 min at a discharge voltage of 750 V, while for Ra~280 nm the exposure time was increased to 90 min and the discharge voltage to 850 V [10]. An example of AFM topographical maps for a sample with surface roughness of 110 nm (Mo 065) is presented in Figure 1a. From this AFM data, we can determine the height distribution of the samples surface, shown in Figure 1b and also the distribution function of surface angles, shown in Figure 1c. To produce samples with an even higher surface roughness above 1 μm, the substrate was sandblasted with glass spheres, using a driving pressure of 3 bar. To determine the surface roughness of this sample type, we performed CLSM on the finished sample after texturing and Mo coating. The obtained surface roughness was in the range of Ra~2-3 μm, with some significant variation between samples and different points on sample.

The prepared substrates were coated with a thin film of Mo (thickness 115-120 nm), using pulsed laser deposition in vacuum. The laser fluence was 2 J/cm^2 and the deposition time 11 minutes. Thanks to the high energy of impinging species, the deposited films mimic the surface morphology of the treated substrate while ensuring a good adhesion. A uniform coverage of Mo over the whole sample surface was obtained by rotating the substrate holder. The uniformity of the Mo coatings was checked by SEM and RBS with ^{4}He ions before exposure to D ion irradiation. In figure 2, we show the SEM images of graphite substrates for a polished, for one of the intermediate roughness steps and for a 2-3 µm rough surface, before and after coating it with Mo. From the presented data, we can conclude that the coverage of Mo is rather uniform and that the deposition has not significantly altered the surface morphology of the substrates. The RBS spectra support this conclusion as no change in the low energy shoulder of the Mo peak is visible.

The chosen exposure fluence of D ions for the sputter yield measurements was sufficiently low that D ions did not introduce additional features on the samples. This can be seen in Figure 3 showing CLSM microscopy images as well as surface height for the sample with a 2-3 µm roughness for both the virgin sample and after the D ion exposure in the centre of the sputtering crater. No apparent differences show up, considering that in the extreme cases we erode 1/3 of the original Mo layer thickness.

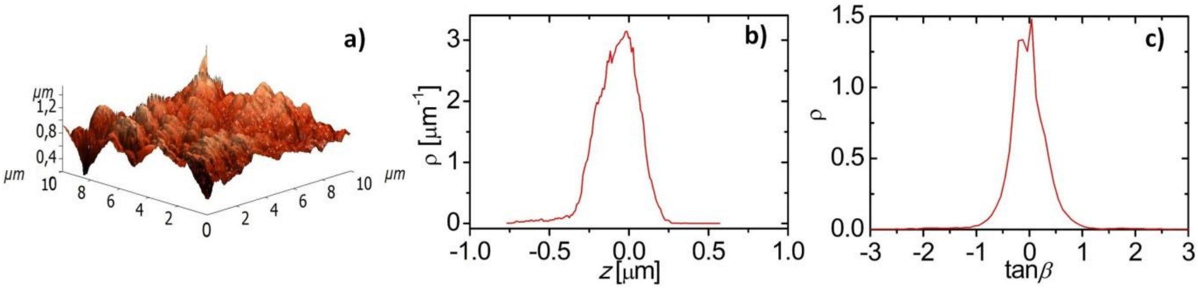

Figure 1: AFM image of Mo 065 sample with surface roughness of Ra~110 nm (a). From AFM images we extracted distribution density - ρ for height -z (b) and slope angles - β (c), respectively.

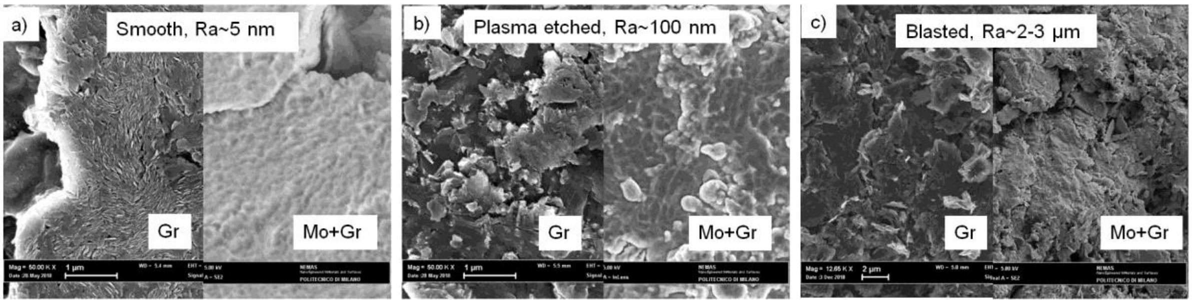

Figure 2: SEM images of secondary electrons from graphite samples with surface roughness (a) 5 nm, (b) 110 nm and (c) 2-3 µm after surface treatment. The left images show the graphite substrate (Gr) and right ones after the deposition of ~120 nm Mo coating (Mo-Gr).

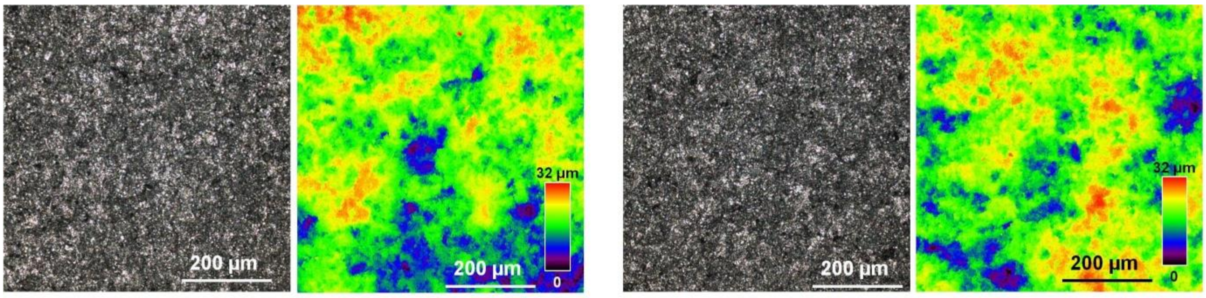

a)

b)

Figure 3: CLSM images of a sample with a surface roughness of Ra~2-3 µm (sample Mo 075). a) virgin sample, b) near the centre of the sputtering crater after D ion exposure. Left is the composite light image of z scan, right is the height distribution of the surface.

All the samples were analysed by RBS using a ^{4}He ion beam at 2.5 MeV before and after exposure to the D ion beam. From RBS, the areal density of the Mo layer can be obtained, which is often for convenience transformed into an equivalent layer thickness value using the theoretical Mo bulk atomic density. We used the SIMNRA software [11] to obtain the areal density. All measurements were performed in the INSIBA experimental chamber coupled to the 2 MV tandem accelerator at Jožef Stefan Institute (JSI) [13]. For the detection of the backscattered He ions in the RBS measurements, we used a Passivated Implanted Planar Silicon (PIPS) detector installed at 165° scattering angle with a circular aperture with a diameter of 5.7 mm, corresponding to a solid angle of 0.689 msr. The schematic representation of the RBS measurement set-up is shown in Figure 4b. The deposited dose of ^{4}He ions was controlled by integrating the beam current on a mesh charge collector mounted between the collimating slits and the sample [12]. With the ^{4}He probing beam, we performed a lateral scan in the middle of the sample in the direction of the rotation axis to avoid geometric effects of the D beam projection on the sample at different impact angles. For the RBS analysis, we used a probing beam with a diameter of 1 mm. The measurements were performed in 2 mm lateral steps.

3. Experimental set-up for sputter yield measurements

We designed a special experimental set-up to perform the study of sputter yield as a function of the impact angle. This set-up was mounted inside the INSIBA vacuum chamber [13], where a newly constructed sample holder was mounted for this study. This holder allows rotating samples up to 90° with respect the ion beam axis, where the vertical Z axis on the sample is our rotation axis. The normal of the sample is defined as Y axis and together with the axis of the ion gun they define the impact angle of the ion beam. The experimental set-up is schematically represented in Figure 4a.

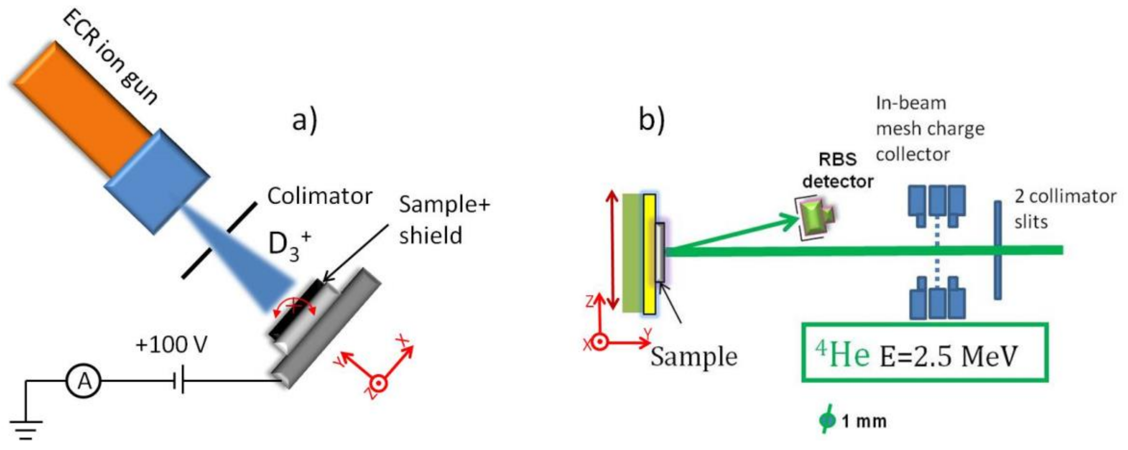

Figure 4: Top views of experimental set-ups for a) D ion irradiation at different impact angles (rotation axis represented by red cross) and b) RBS measurement for characterisation

of samples (scanning direction marked by red arrow is along rotation axis in a)). Both set-ups can't be installed in the INSIBA experimental chamber simultaneously, therefore we had to use them interchangeably [13].

Additionally, we added a special shield for the side faces of the samples. The shield was made of stainless steel to prevent unintended sputtering of the edges of the graphite substrate at higher impact angles and redeposition of carbon on the Mo surface. A commercial Electron Cyclotron Resonance (ECR) ion gun (IonEtch Gen II made by Tectra GmbH) was used as a source for the keV D ions. The ECR ion source uses microwaves at a frequency of 2.45 GHz to excite gas inside the plasma chamber surrounded by rare earth permanent magnets providing the magnetic field to maintain the plasma in the chamber. The ions are accelerated by applying a voltage to the extraction electrode in the excitation chamber. In our experiment we used D_2 feeding gas to produce D ions. To run the D plasma, the pressure in the INSIBA vacuum chamber typically increased to 30 mPa nitrogen equivalent. At such conditions, the dominant species extracted from the plasma chamber are D_3^+ (about 93 %) [12]. The ion flux was monitored by measuring the ion current on the sample during the exposure experiment. To suppress secondary electrons escaping from the sample, the rotatable sample holder was biased to +100 V. The positive extraction voltage of the ion gun was adjusted to 3.1 kV resulting in an ion energy of 3 keV. We assume that for molecular ions (D_3^+, D_2^+) the energy is shared evenly between the D atoms upon contact with the sample surface. Thus, the D flux is nearly three times larger than the measured ion flux and we refer to these conditions as 1 keV/D for the majority D_3^+ ions impacting on the surface.

The D ion beam at the exit of the ECR gun has a large angular divergence, which is energy dependent. For our applied extraction voltage of 3.1 kV, the beam average divergence angle is ⍰ 30° [14]. Due to a relatively large distance between the sample and the

ECR ion gun exit aperture of 33 mm, a large fraction of the beam would not only hit the sample but also the supporting structure of the rotating table. In this case, we would still measure these ions as ion current, while they would not contribute to the erosion of Mo and consequently overestimate the real sputter yield. To overcome this issue and to produce a well-defined ion beam size at the sample position, we inserted a molybdenum collimating aperture of 2.7 mm in diameter between the ECR source and the sample, which is positioned between the source and the sample, 28.2 mm in front of it. This reduced the beam diameter to a value below the lateral sample size at 0° impact angle. Since at higher impact angles the beam diameter is geometrically enlarged, still a part of the beam misses the sample. Due to well-done calibration of the ion gun output, the ion current measurements during the exposure were only used to control the stability of ion gun output over the time of exposure, as it can drift over longer times due to change of the pressure in plasma chamber of the ion gun. The ion fluence at the RBS analysing position was calculated from the average ion gun output as measured during the calibration process.

The ion beam size and the profile at the sample position were measured by two independent methods. One was by eroding a thin film of amorphous hydrocarbon (a-C:H) layer on silicon. The beam size and the erosion crater were derived by optical interference of the light on the thin film as seen in Figure 5a.

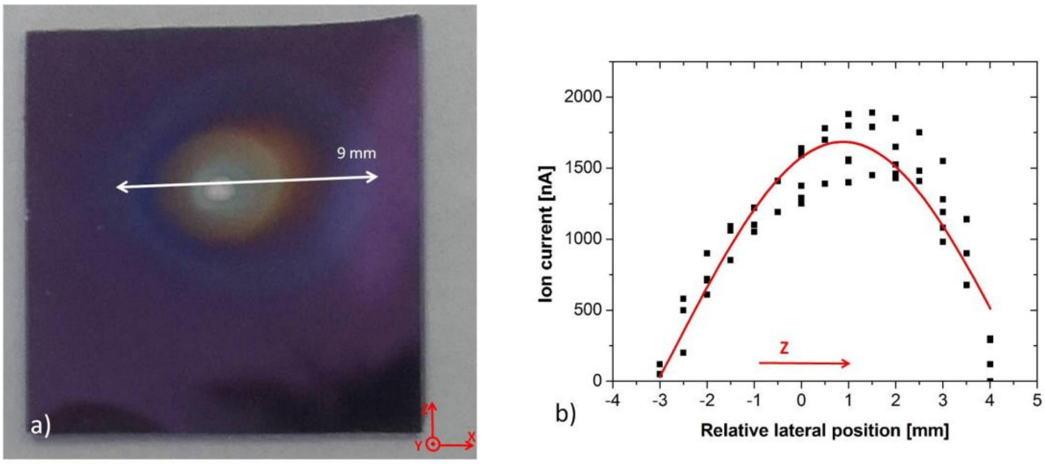

Figure 5: a) Image of the erosion crater, created by 1 keV/D ions, as seen on a thin a-C:H film on silicon. b) lateral profile along the sample rotation axis of the 1 keV/D ion beam as measured using a Faraday cup with a 2 mm aperture. Due to geometrical constraints in the experimental chamber, the distance from collimator to the Faraday cup aperture is reduced to 20.2 mm instead of 28.2 mm where the surface of exposed samples was later positioned.

Secondly, we carried out lateral scans of the ion current with a Faraday cup along the Z axis. The results of the scans are shown in Figure 5b. The Faraday cup had an entrance hole of 2 mm in diameter and the current measurements were made at a distance of 20.2 mm from the collimating aperture, instead of 28.2 mm where surface of the exposed samples was. By the Z axis scans we confirmed that 90% of the total ion current is within a nominal beam diameter of 6.7 mm. If one corrects the difference in the distances between the Faraday cup during the current measurements and the a-C:H sample, we obtain a value of 9.4 mm for the beam diameter at the sample position. Both methods give a good agreement in D ion beam size, which we estimate to be 9 mm in diameter. The ion beam exhibits a truncated Gaussian profile. The central maximum of the D ion beam flux was determined to be 8×10^{18} D ions/m^2 s with the Faraday cup measurements. By averaging the ion flux as measured by the Faraday cup over the entire irradiated area, we end up with an average flux of around 3×10^{18} D ions/m^2 s. The total D ion current impinging on the sample was measured during the irradiation with a Keithley 2000 multimeter. The time average fluence per sample was calculated as the time integral of the D ion current divided by the beam area and elementary electron charge and multiplied by three due to the D_3^+ ions. This laterally averaged fluence is suitable to compare experiments during the exposure and for monitoring the stability of the D ion beam. However, to derive the sputter yield the maximum fluence of the exposure spot was used and compared with the maximum erosion derived from RBS as will be explained in the result section.

4. SDTrimSP-3D simulations

The angle-dependent sputter yield measurements were compared with static SDTrimSP-3D [9] simulations based on the sample surface morphology extracted from AFM scans and CLSM microscopy. For samples with intermediate roughness AFM measurements on 10×10 µm^2 grid with lateral resolution of 39 nm and high resolution of less than 1 nm. For the roughest samples surface height measurements performed with CLSM microscope on 650×650 µm^2 grid with lateral resolution of 625 nm high resolution of less than 100 nm. Those data were used as input for SDTrimSP-3D simulations with linear interpolation between measuring points to match the surface cell density in SDTrimSP-3D grid with periodic boundary conditions.

5. Results and discussion

5.1 Experimental results

The samples were irradiated with a maximum fluence of the exposure spot ranging from 0.85 to 3.19 $\times$ 10^{23} D ions/m^2 at different impact angles of 0°, 40°, 60° and 70°. A detailed list of irradiation parameters for each individual sample can be found in Table 1. Initially it was planned to erode 10-20 % of the initial layer and we calculated that for this we would need a fluence of approximately $2 \cdot 10^{23}$ D ions/m^2. However, since we expected a strong dependence of the sputter yield on the exposure angle [2, 4] we needed to adjust the exposure fluence for some exposure conditions not to erode too much of the initial layer. Still, due to the large variation of the sputter yield in some cases up to 50 % of the initial layer was eroded. Besides this upper limit for the D fluence we kept a lower fluence limit for all irradiations. Recent experiments showed a fluence dependent sputter yield for D ion irradiation of iron [6]. However, the effect becomes noticeable only at fluence values below 10^{22} ions/m^2 and can be attributed to the presence of oxides at the surface. For monoelemental surfaces without surface oxide layer, this threshold fluence should be even lower, as shown for iron targets [15]. For this reason, we assume that the different exposure fluences applied in our experiment on different samples do not significantly influence the obtained sputter yield values.

Sample	Treatment	Ra [nm]	Angle [°]	Maximum fluence [*10^{23} D/m^2]	Sputter yield [*10^{-2}Mo/D]
Mo061	Polishing	~5	0	2.67	0.6±0.15
Mo062	Polishing	~5	40	3.19	1.0±0.3
Mo063	Polishing	~5	60	2.53	1.6±0.60
Mo064	Polishing	~5	70	1.39	2.5±1.0
Mo065	Plasma etching	~110	0	2.46	0.5±0.1
Mo066	Plasma etching	~110	40	1.84	1.1±0.3

Mo067	Plasma etching	~110	60	1.27	2.1±0.8
Mo068	Plasma etching	~110	70	0.86	3.3±1.3
Mo070	Plasma etching	~280	0	2.46	0.8±0.2
Mo071	Plasma etching	~280	40	1.76	2.2±0.5
Mo072	Plasma etching	~280	60	1.32	3.2±1.3
Mo073	Plasma etching	~280	70	0.89	2.9±1.2
Mo076	Sand blasting	2-3 µm	0	0.85	1.3±0.3
Mo075	Sand blasting	2-3 µm	40	1.25	0.95±0.2
Mo074	Sand blasting	2-3 µm	60	1.92	0.5±0.2
Mo059	Sand blasting	2-3 µm	70	2.5	0.3±0.10

Table 1: *Exposure parameters for each individual sample. All samples were exposed to D ion beam with an energy of 1 keV/D at 300 K. We list here the sample naming, treatment of the substrate surface, estimated surface roughness, angle of incidence of the D beam, the maximum fluence of the exposure spot where RBS analysis was performed and calculated sputter yield as described in the text.*

After the exposure of each series of samples to the D ion beam, they were analysed by RBS. By comparing the measured Mo thickness profiles obtained by RBS before and after exposure to the D beam, we can determine how much of the material was eroded at a certain D ion fluence. An example of an RBS measurement before and after D exposure is shown in Figure 6 where one sees a Mo peak at around 2.1 MeV and RBS signal from the carbon bulk material at lower energies. It is clearly visible that the Mo peak integral becomes smaller after the D ion irradiation compared to the virgin sample. This shows that the Mo layer was considerably eroded by the D ions.

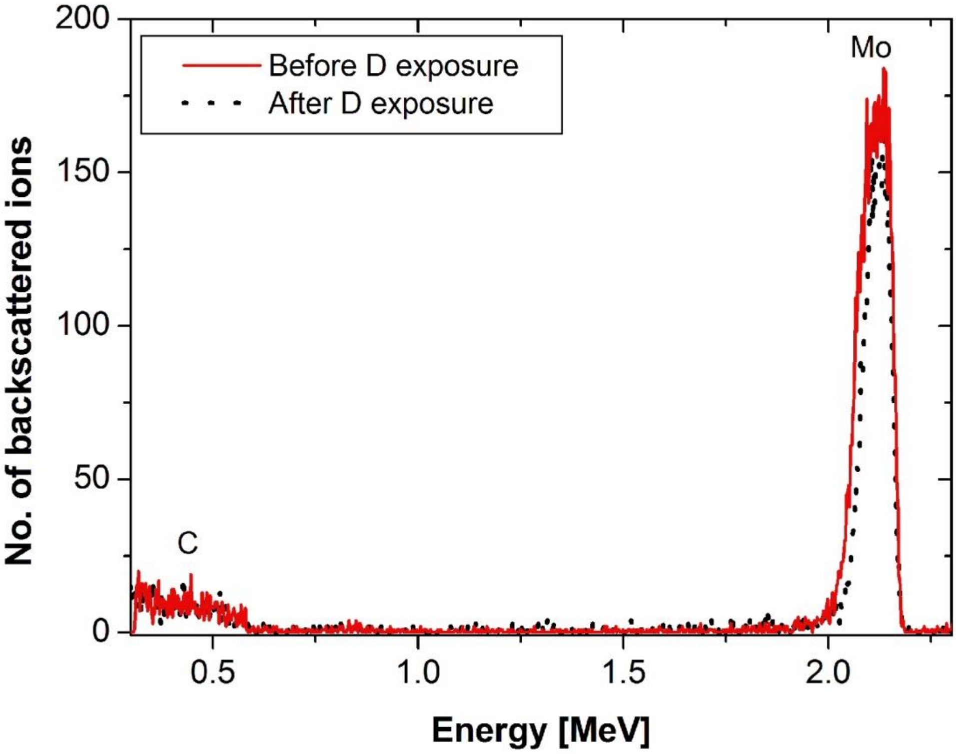

Figure 6: Spectra of RBS measurements of a Mo-coated graphite sample (roughness 5 nm) using 2.5 MeV ^{4}He ions, before and after the exposure to 1 keV/D ions at 0° in the middle of the erosion crater.

In Figure 7 we show the vertical profile scan of the nominal Mo layer thickness before and after the D ion exposure as measured by RBS. We see that the thickness of the virgin Mo layer is within 5 % of the nominal thickness of 115 nm or 7.4×10^{17} Mo/cm^2, respectively. This number is only given as an orientation but since we were aware from previous experience that samples could have some variance in thickness and gradient along the sample, each sample was measured before the ion exposure. For this reason, we took for the sputter yield calculations as the initial thickness the value measured in the middle of the sample with the variation from few neighbouring positions. In addition to the RBS measurement, the Gaussian approximation of the beam profile is also shown in figure 7. The minimal nominal layer thickness after the D ion exposure coincides well with the maximum of the beam. In some cases, we observe some decrease in the Mo layer thickness outside the centre of the beam. We think this is due to D ion beam halo, which can be observed also on eroded a-C:H film, Figure 5a.

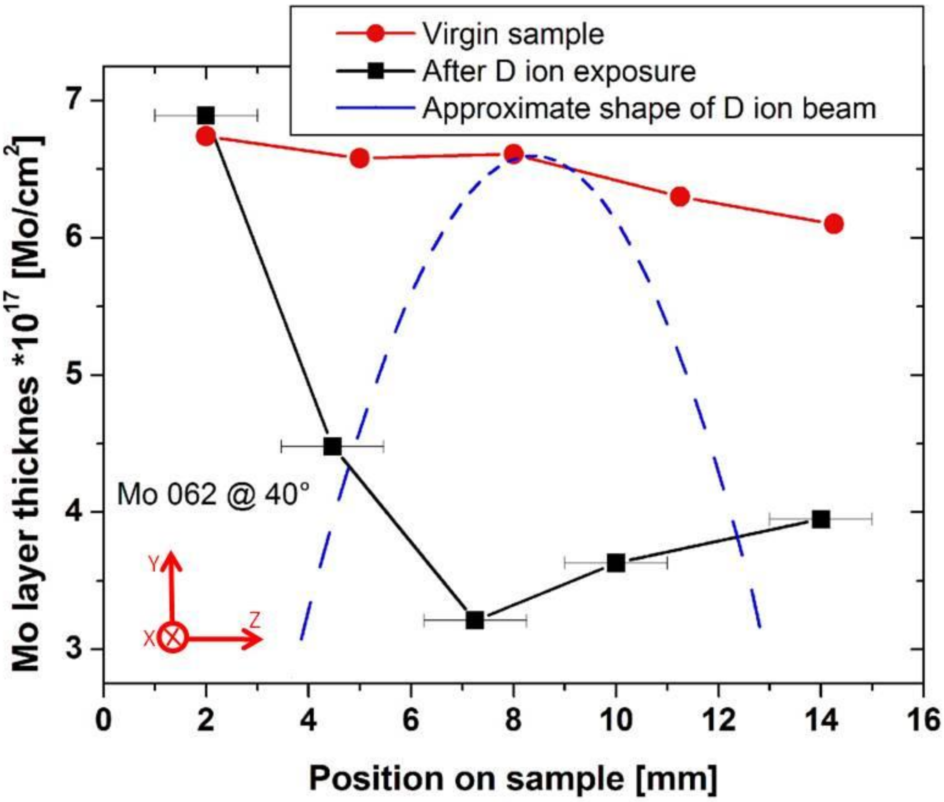

Figure 7: Thickness of the Mo layer as measured by RBS, before and after the exposure to 1 keV D ions at 40° impact angle on smooth sample with Ra~5 nm. The dashed line represents the envelope of the ion beam, approximated by a Gaussian fit of the Faraday cup measurements from Figure 5. The error bars on individual positions represent the error of position between before and after exposure RBS measurement. Due to high fluence on this sample $D_{max}=3.19\times10^{23} D/m^2$*, the depression in erosion crater exceed the 50% of the original Mo thickness.*

The difference between the Mo areal density $n_{Mo(before)}$ of the initial layer and the areal density $n_{Mo(after)}$ of the irradiated surface gives us the amount of eroded Mo atoms. Sputtering is quantified via the sputtering yield, which is defined as:

$$Y_{Mo} = \frac{n_{Mo(before)} - n_{Mo(after)}}{D_{fluence-max}}.$$

$n_{Mo(before)}$ was taken as an average of five measurement points across the sample, while $n_{Mo(after)}$ was taken at the minimum Mo thickness measured at the bottom of the erosion crater (see Figure 7). In the centre of the sputtering crater we have also estimated the maximum D ion fluence, marked as $D_{fluence-max}$. The value of $D_{fluence-max}$ was calculated by multiplying the time-averaged D ion fluence as measured during individual sample exposure, given in table 1, by the ratio of 2.7 and cosine of the angle between sample surface normal and ion gun axis.

D irradiation and RBS analysis had to be conducted with two different sample holders inside the INSIBA chamber. Therefore, the samples had to be transferred from one holder to the other, which could result in the worst case to a mismatch of measuring position fore ~1 mm, i.e., the maximum of the erosion crater is missed by 1 mm, while still the maximum of the D ion flux is used for calculating the sputter yield. This corresponds to an overestimated $D_{fluence-max}$ by 15%, which translates to underestimation of the sputtering yield by 15% at 0° impact angle and up to 30% at high impact angles. Hence, we assume that the estimated mismatch gives us the dominant contribution to the error bars for our absolute values of the sputtering yields. To the error bars being due to the possible mismatch of the maximum erosion crater we have added also the errors due to the RBS measurements statistics and the discrepancy between the measurements and the simulation in the SIMNRA software. This adds additional 5 % error to the calculated sputter yield. The dose measurement is not included in the error since it is a systematic error and is estimated to be about 5-10 %.

Figure 9 shows the sputter yield as obtained for the smooth surface with Ra~5 nm. We observe a clear increase of sputter yield with increasing angle of incidence by roughly a factor of five at 70° as compared to 0°.

The experimental results for the all four investigated surface roughnesses are presented in Figure 10, which shows the sputter yield as a function of impact angle together with SDTrimSP-3D simulations for the specific surface roughness. For easier comparison, the 5 nm roughness case is also shown in Figure 10a, the same data as in Figure 9. For all the surfaces we observe a strong angular dependence of sputter yield. Intermediate surface roughnesses, i.e. Ra~110 nm and Ra~280 nm, show an increase of the sputter yield with the angle by a factor of approximately five compared to 0^o, reaching similar values as Ra~5 nm. - For the smooth surface with Ra~5 nm and the low roughness surface with Ra~110 nm, there is no maximum observed in the analysed angle range and the yield increases up to the highest measured impact angle of 70^o. For the surface roughness of Ra~230 nm, the maximum of the sputter yield is observed at 60^o. For Ra~2-3 µm there is no increase of sputter yield for large angles but it attains its maximum at 0^o. The sputter yield at 0^o shows an increase with surface roughness from 0.5×10^{-2} Mo/D for the low values of Ra to 1.3×10^{-2} Mo/D for the roughest surface. The sputter yield at large angles, e.g. at 60^o, increases with the surface roughness except for the case of h highest roughness studied, where it attains the lowest value.

5.2 Simulation results

Figure 8 also includes the results obtained by applying the semi-analytical fit formula from [2] and simulated data computed by SDTrimSP-1D [17] and -3D [9]. The semi-analytical formula is only valid for smooth surfaces. The input parameters used are: f=1.66, b=0.328, c=1.015, $Y(E_0,0)=0.015$. The parameters were extrapolated from Table 20 in *R. Behrisch and W. Eckstein* [2], as there are no parameters for a D ion energy of 1 keV on Mo. Simulations by SDTrimSP were performed with 10^6 projectiles. Surface binding energy E_s was set to 8.45 eV. The heat of sublimation $\triangle H_s$ is a first-order approximation for E_s being 6.81 eV [16]. Comparisons of calculated and measured energy in literature have led to argue that, at least in the case of Mo, E_s is larger than the heat of sublimation [16]. For this reason, an average value of the surface binding energies for different surface orientations, as they range from 7.38 eV up to 9.18 eV [16], was used in the calculation. A lower value of surface binding energy leads to higher values of sputter yield for all angles.

One of the main input for SDTrimSP-3D is the morphology of the surface. This information was derived from AFM (Ra~ 110 nm and 280 nm) as well as CLSM (Ra~2-3 µm) measurements. However, for the samples with Ra~5 nm, the observed holes (artefacts of polishing as discussed in sample preparation section) could not be measured accurately with the AFM, since the depth of the holes is larger than the dynamic range of the AFM. Therefore, the input surface for SDTrimSP was constructed as smooth surface with one cubic depression with dimensions of 2.5×2.5×2.5 μm^3, on the 10×10 μm^2 grid, thus creating an uniform distribution of holes on simulated surface. Such a construction matches the surface morphology observed by SEM and produces good agreement of the SDTrimSP-3D calculated sputter yield with the measured ones. We also tried the simulation with different hole dimension, as seen on figure 8, which yielded similar absolute values of the sputter yield. Thus, we did not proceed further with simulation of uneven distribution of hole size. This construction was chosen because using only AFM data as input for the surface structure could not reproduce the surface.

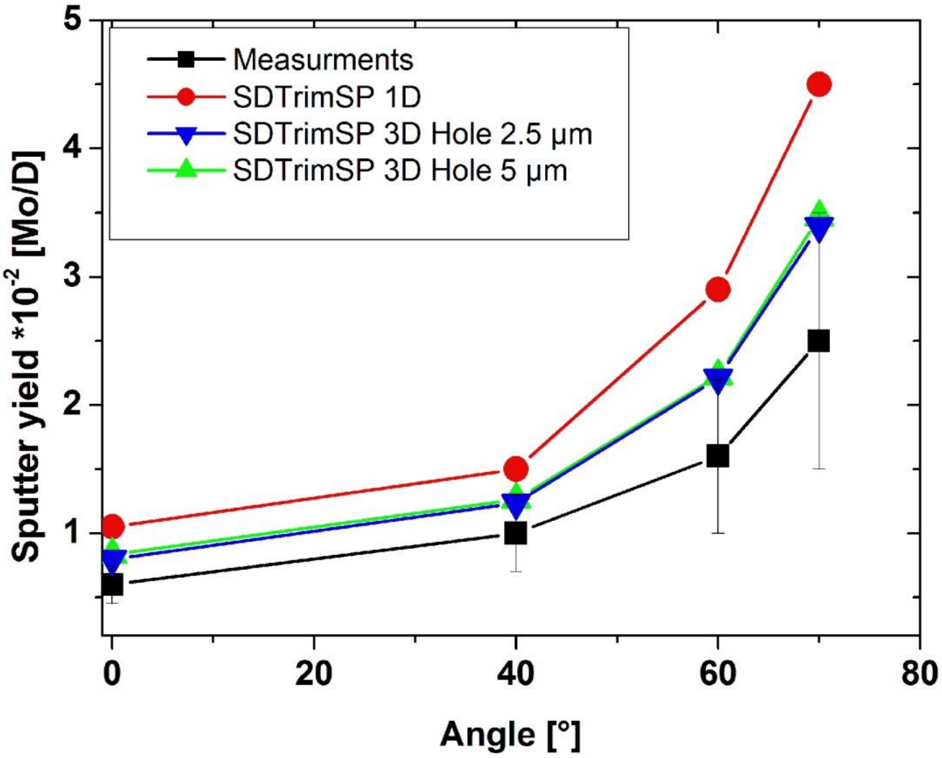

Figure 8 Angular dependence of the Mo sputter yield for 1 keV D particles for samples with Ra~5 nm. Additional to the experimental values, the yields obtained with SDTrimSP 6.0 code [17] and with SDTrimSP-3D [9]. For SDTrimSP-3D we plotted the simulations for holes of 2.5 µm and 5 µm.

Comparison of the SDTrimSP-3D simulated data with experimentally measured data shows that simulations give slightly higher values of the sputter yields, but are still within the experimental error bars. Also the semi-analytical formula and SDTrimSP-1D lead both to larger values as compared to the experimental data. However, all three approaches agree on the trend of the sputter yield dependence on the impact angle, namely that the sputter yield increases drastically for angles above 50°.

The simulation data obtained from SDTrimSP-3D for all the studied surface roughnesses are shown in figure 10. For intermediate surface roughness, we did not observe this micron-size holes as seen on polished samples. Therefore, we did not include additional holes in calculations for other surface roughnesess. We are suspecting that plasma etching procedure to smoothens out the holes to some extent. The trend of the simulated sputter yield with increase of the angle agrees with the experiment for the surface roughness of 110 nm. In the case of 280 nm surface roughness, the simulation does not show any peak of sputter yield at 60° as is observed in experimental data but just increases with angle as for the other two cases before. The simulation for the roughest surface of 2-3 µm predicts an increase of the sputter yield by a factor of 1.5 at the largest angle, while the experimental data show a decrease of the sputter yield by a factor of five. The absolute values of the simulated sputter yield at 0° are in all cases higher than in the experiment except for the roughest case.

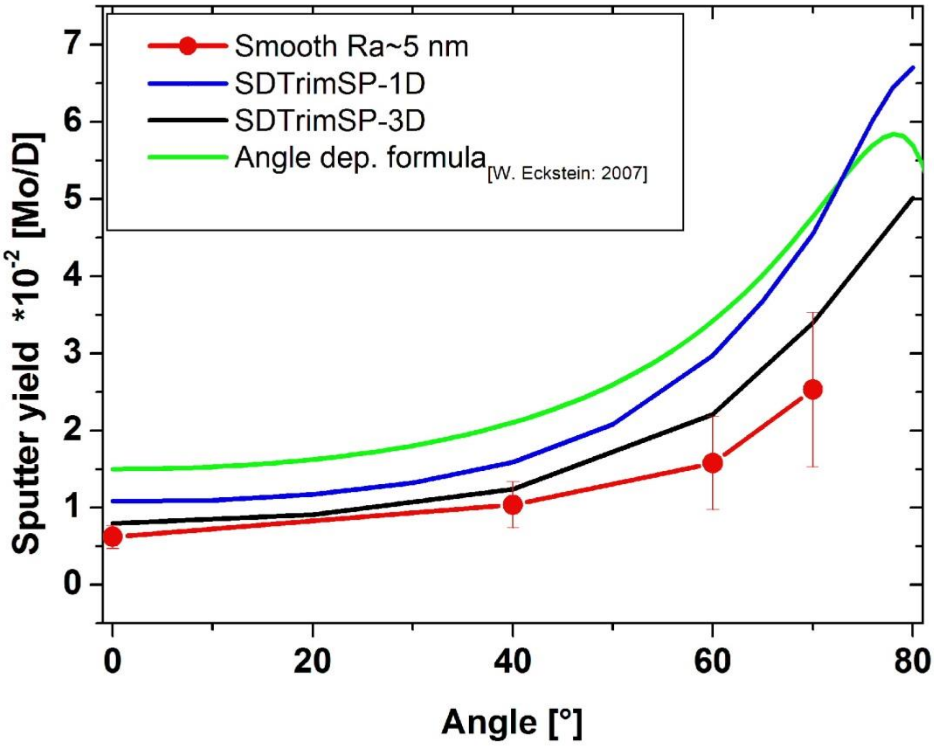

Figure 9: Angular dependence of the Mo sputter yield for 1 keV D particles for samples with Ra~5 nm. Additional to the experimental values, the yields obtained with SDTrimSP 6.0 code [17] and with SDTrimSP-3D [9] as well as the ones from a calculation using the Eckstein angular formula [2] for ideal smooth surfaces are given.

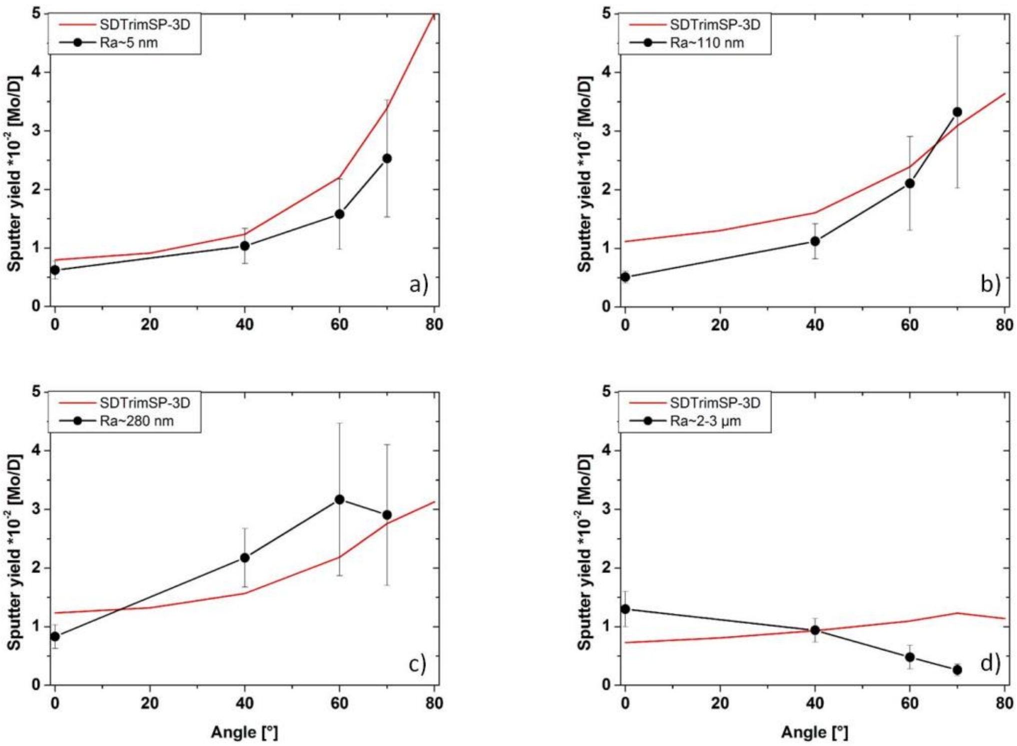

Figure 10: The experimental sputter yield and the SDTrimSP-3D simulation results as a function of angle for 1 keV D on Mo for the four different studied surface roughness with Ra a) ~5 nm, b) ~110 nm, c) ~280 nm and d) ~2-3 µm.

5.3. Discussion

We will first discuss the quality of the agreement between the experiment and the simulation. Second discuss the possible reason for disagreement of both data. In Figure 11 we show the relative values of the measured sputter yield divided by the values calculated with SDTrimSP-3D. If simulations are in total agreement with the measurements, we expect flat lines in the vicinity of 1. This is the case for the smoothest samples with Ra~5 nm, obtaining almost perfect agreement with only systematically overestimating the simulated sputter yield. With increasing surface roughness a larger deviation between simulation and experiment is observed. However, except for Ra~2-3 µm, the general trend with angle of incidence can be seen in both cases.

In general, the SDTrimSP-3D calculations give lager values as measured. For the case of the samples with Ra~2-3 µm, larger discrepancies between the calculated and the measured data can be noticed. As shown for the case of SDTrimSP-3D calculations for smooth surfaces, we needed to introduce the surface with holes to calculate the sputter yields. As compared to the 1D model, the introduction of holes significantly decreases the sputter yield [18]. The surfaces for the roughest samples also show some deep depressions in the surface morphology and these were fed in SDTrimSP-3D as input. This is one of the possible reasons to obtain lower values of sputter yield. Additionally, SDTrimSP-3D does not take into account spikes smaller than the lateral resolution of the input data. In our case this means no additional features smaller than 650 nm. From SEM images, seen on figure 2, we observe structures, with smaller Ra, on top of the rough surfaces. The erosion of these spikes-like structures can explain the larger values measured at 0° impact angle compared to simulations. In addition, these structures increase the active surface of the sample. This leads to a larger prompt deposition rate at higher impact angels, which is experimentally observed as a decrease of the sputter yield. From SDTrimSP data we can estimate that this prompt deposition can occurs for up to 25% of sputtered atoms. However, the exact value is strongly dependant on surface roughness and impact angles. Despite this the SDTrimSP-3D can still be a useful tool to predict the behaviour of the sputter yield. However, we need to be aware of its limitations posed by the quality of the provided input data, provided with CLSM.

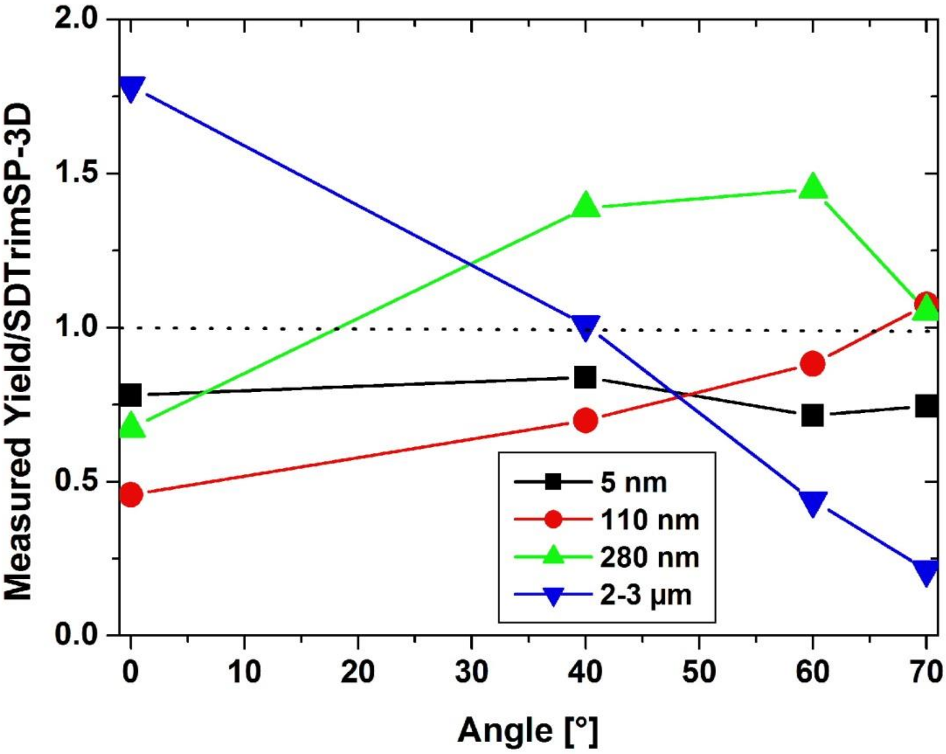

Figure 11: Measured values of the sputter yield divided by the SDTrimSP-3D calculated values. As observed in most of the cases the SDTrimSP-3D calculation of the sputter yield is higher than the experimentally obtained sputter yield.

From the presented data we can observe that the surface roughness influences the sputter yield differently at small and large impact angles. Let us first consider large incidence angles. For the polished samples and samples of intermediate roughness, we can see an increase of the sputter yield with increasing impact angle, dominantly for angles beyond 40°. This trend is also supported by SDTrimSP-3D simulations. As for angles between 0-40° we do not have data, it is only a speculation how sputter yields behave in this range. The increase of sputter yield with higher impact angles can be easily explained by the fact that more momentum is transferred to target atoms in the forward direction. Therefore, the probability of atoms escaping from the surface increases at larger impact angles. With such a model we would see the maximum sputter yield for smooth surfaces at angles approaching 90°, which is also supported by theoretical prediction of Eckstein [2]. As the surface roughness increases, more of the surface elements are exposed at effectively larger angles (90°). The consequence of the change of the effective impact angle with increasing roughness can be observed by the fact that the steepness of the angular dependence the sputter yield is decreasing, as observed by the experiment and confirmed by simulation.

When we increase the surface roughness to larger values, two additional processes start to affect the sputtering process. The first process is local redeposition of sputtered atoms on the nearby surfaces. This increases the probability of a sputtered atom remaining on the surface, which decreases the measured sputter yield. From our design of the experiment, we only detect the atoms sputtered away from the target and none of the sputtered atoms that are promptly redeposited at the surface. The second process is that the increase of surface roughness also leads to shadowing effects, which are more pronounced at higher impact angles. Therefore, less sample surface is exposed to the irradiating D beam, which leads to a corresponding decrease of the sputter yield. An illustration of these two processes is schematically shown in Figure 12. From our results we assume that these two effects are most pronounced for the samples with the highest surface roughness (2-3 µm). To make clear conclusions, more intermediate roughness values should be investigated. In any case, we see that the sputter yield is significantly deceasing for higher impact angles as compared to 0° impact angle for rough samples.

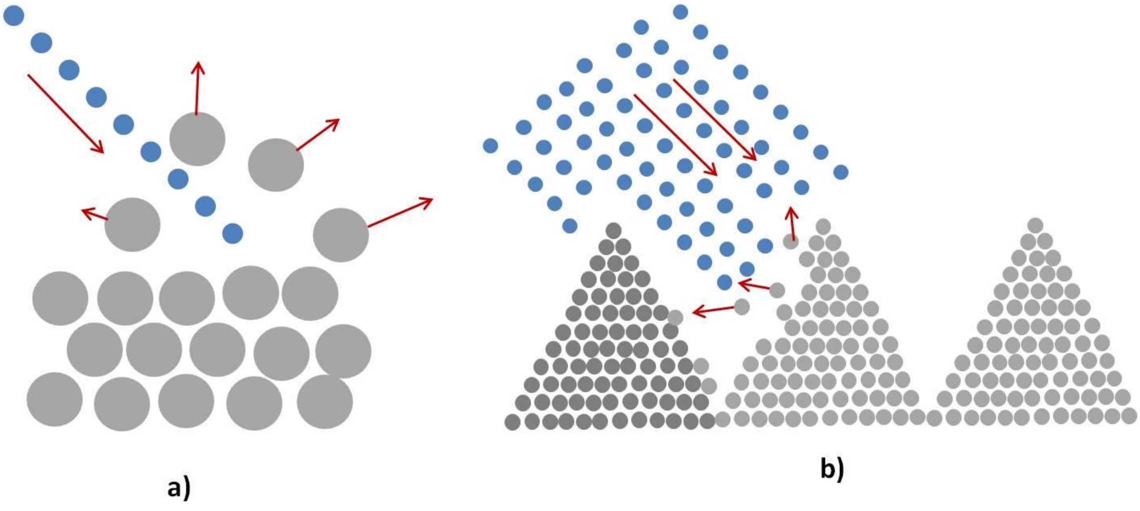

Figure 12: *Schematic representations of the processes competing and providing the angular and roughness dependence of the sputter yield. a) Transfer of momentum in lateral direction at higher impact angles for smooth surfaces. b) Rough surfaces increase redeposition of sputter atoms and shadowing of surfaces.*

Now let us discuss about the discrepancy in the sputter yield between the measured and the simulated values at low impact angle where we also measured a small increase with surface roughness for surface rougnesses of ~280 nm and ~2-3 µm. A similar behaviour of the absolute sputter yield values compared to SDTrimSP simulations for different surface roughness was observed by Arredondo et al. [5]. They also report an increase of the sputter yield at low impact angles (<40°) with increasing surface roughness and decrease at high impact angles (>40°). It is important to stress that the rough surfaces prepared in that experiment had a much wider angular distribution of surface angles compared to the samples in our study, although they still had a Ra value of 20 nm. This angular distribution in case of Arredondo et al. [5] is assumed to be the origin of the lower sputtering yield at 60° impact angle compared to the smooth surface, despite the low Ra value. We observe an increase of the sputtering yields for intermediate roughness. One of the most important issues raised by R. Arredondo et al. [5] is the observed discrepancy of calculated sputter yields with SDTrimSP [9] for D on W, where SDTrimSP overestimated the sputter yield approximately by a factor of two. The explanation given by Arredondo et al. [5] is that the binary collision approximation, on which SDTrimSP code is based on, is not strictly satisfied for brittle materials (W, Mo), in contrast to ductile ones (Ni, Au). We observe a similar overestimation for D on Mo, where the simulated or literature data [2] exceed the measured sputter yield, Figure 9. The agreement between experimental data and SDTrimSP-3D simulations was improved by taking a higher surface binding energy and appropriate surface morphology data. With this the simulations achieved better agreement with the measured data.

6. Conclusion

The aim of this work was to investigate the effect of surface roughness and morphology on the sputter yield of Mo. To this end a series of Mo thin film samples of varying surface roughness were exposed to D_3^+ ions with 1 keV/D ions at room temperature under different impact angles ranging from 0 to 70°. The experimental results were compared to SDTrimSP 1D and 3D simulations.

The data obtained in this study reveal that there is a clear influence of the incidence angle and surface roughness on the sputter yield of Mo. For polished surfaces we observed an increase of the sputter yield at higher impact angles, as predicted by theory. With increasing surface roughness, the sputter yield increases at 0° impact angle. For higher impact angles we observe two different behaviours: if the surface roughness is in the medium range experimentally investigated (a few hundreds of nm), the dominant effect is that more and more surface is exposed to higher impact angles leading to correspondingly increasing sputter yield. However, for the very rough surfaces a decrease of the sputter yield at high impact angles was observed which we explained by redeposition and shadowing effects of the rough surface. As we showed, this decrease is only observed on surfaces with the highest surface roughness of 2-3 µm.

In general, the calculation with SDTrimSP-3D qualitative produce good agreement with measured angular and roughness dependence of sputter yield. However, there are still discrepancies between the absolute calculated values of sputter yield with SDTrimSP-3D code and measured values. The possible reason for this is the lack of necessary detail in surface reproduction which is not possible with current methods but a necessary input for SDTrimSP-3D. Therefore, we infer that for now it is more advisable to take experimental data for PFC design works on surfaces as they more closely resemble the real components.

The simulated conditions of irradiation with mono-energetic D and fixed angles represent a compromise between well-characterised ion beam and real conditions in a thermonuclear reactor, where we have a broader distribution of particle energies and also the local magnetic field exerts a strong influence on the effective impact angle [16]. Still, the obtained data serve as a valuable guideline for the design of plasma-facing component surfaces in tokamaks and for estimating their lifetime. Strictly from the erosion point of view, the components with high value of Ra will last longer than smooth ones.

Acknowledgments

This work has been carried out within the framework of the EUROfusion Consortium and has received funding from the Euratom research and training programme 2014-2018 under grant agreement No 633053. Work was performed under EUROfusion WP PFC. The views and opinions expressed herein do not necessarily reflect those of the European Commission. The authors acknowledge the support from the Slovenian Research Agency (research core funding No. P2-0405).

References

[1] R. Chodura, Journal of Nuclear Materials. 111 (1982) 420-423

[2] W. Eckstein. Sputtering yields. In R. Behrisch and W. Eckstein, editors, Sputtering by Particle Bombardment IV, volume 110 of Topics in Applied Physics, chapter Sputtering Yields, pages 33–187. Springer Berlin Heidelberg, Berlin, 2007.

[3] M. Küstner et al. Nuclear Instruments and Methods in Physics Research B 145 (1998) 320

[4] M. Küstner et al. Journal of Nuclear Materials 265 (1999) 22

[5] R. Arredondo et al. Nuclear Materials and Energy 18 (2019) 72

[6] R. Stadlmayr et al. Instruments and Methods in Physics Research B 430 (2018) 42

[7] G. F. Matthews et al. Physica Scripta T145 (2011) 014001

[8] R. Stadlmayr et al. Physica Scripta T171 (2020) 014021

[9] U. von Toussaint et al. Physica Scripta T170 (2017) 014056

[10] E. Vassalo et al. Thin Solid Films 603 (2016) 173

[11] Mayer M 1997 *SIMNRA User's Guide, Report* IPP 9/113,Max-Planck-Instutut für Plasmaphysik Garching (www.rzg.mpg.de/_mam/)

[12] S. Markelj et al. Nuclear Fusion 59 (2019) 086050

[13] S. Markelj et al. Nuclear Materials and Energy 12 (2017) 169–174

[14] IonEtch specification, https://tectra.de/wp-content/uploads/2017/03/IonEtch.pdf (26.05.2020)

[15] B. M. Berger Nuclear Materials and Energy 12 (2017) 468

[16] W. Eckstein, Computer Simulation of Ion-Solid Interactions, Springer Series in Material Science, Vol. 10, Springer Berlin, Heidelberg 1991

[17] A. Mutzke et al. SDTrimSP Version 6.00. IPP 2019-02, Max-Planck-Institut für Plasmaphysik (Ed.) https://pure.mpg.de/rest/items/item_3026474_2/component/file_3026477/content, 2019

[18] A. Mutzke, Personal communication 2020

Author creditship:

M. Kelemen: Conceptualization, Methodology, Writing-Original Draft, Investigation **T. Schwarz-Selinger:** Conceptualization, Writing - Review & Editing **A. Mutzke:** Software, Resources **M. Balden:** Resources, Investigation, Writing - Review & Editing **E. Vassallo:** Resources, Writing - Review & Editing **M. Pedroni:** Resources **D. Dellasega:** Resources, Writing - Review & Editing **M. Passoni:** Resources **F. Romeo:** Resources **A. Hakola:** Conceptualization, Writing - Review & Editing **P. Pelicon:** Resources **R. Zaplotnik:** Resources, Investigation **S. Markelj:** Conceptualization, Methodology, Writing-Original Draft, Investigation, Writing - Review & Editing